Supporting Information

Two-State Nanocomposite Based on Symmetric Diblock Copolymer and Planar Nanoparticles: Mesoscopic Simulation

M.D. Malyshev[1], D.V. Guseva[1], P.V. Komarov[1,*]

[1]A.N. Nesmeyanov Institute of Organoelement Compounds RAS, Vavilova St. 28, 119991 Moscow, Russia
Corresponding author: *E-mail: pv_komarov@mail.ru (P.V. Komarov)

Here we present auxiliary information and a set of additional data not included in the main text of our article.

S1. Dissipative particle dynamics method

In the dissipative particle dynamics (DPD) method [S1–S5], the evolution of the molecular system (composed of a set of DPD particles, hereafter referred to as particles or beads) is determined by integrating the following system of Newton's equations

$$d\mathbf{r}_i/dt = \mathbf{v}_i,\ d\mathbf{v}_i/dt = \mathbf{f}_i, \tag{S1}$$

where $\mathbf{r}_i$ is the radius vector of the i-th particle (the total number of particles in the system is N_{total}), and $\mathbf{v}_i$ is its velocity. We assume that the size of all particles σ, their mass m, and the energy scale factor k_BT in dimensionaless units are equal to 1 (k_B is the Boltzmann constant, T is the temperature), which gives the unit of the time scale $\tau = \sigma(m/k_BT)^{1/2} = 1$. The particles interact with each other through pairwise additive forces $\mathbf{F}_{ij}$, which preserve momentum locally and lead to correct hydrodynamics. The resultant force $\mathbf{f}_i$ acting on the particles is defined as follows

$$\mathbf{f}_i = \sum_{i,i\neq j}^{N_{total}} \left\{ \mathbf{F}_{ij}^{(C)} + \mathbf{F}_{ij}^{(D)} + \mathbf{F}_{ij}^{(R)} \right\} - \partial U / \partial \mathbf{r}_i\ . \tag{S2}$$

It includes three standard DPD forces: a conservative $\mathbf{F}_{ij}^{(C)}$, a dissipative $\mathbf{F}_{ij}^{(D)}$, a random $\mathbf{F}_{ij}^{(R)}$, and an additional conservative force determined by the gradient of the potential energy U described below. In Eq. (S2), the summation is performed for all pairs of particles whose centre distances $r_{ij} = |\mathbf{r}_i - \mathbf{r}_j|$ are smaller than the cut-off radius $r_c = \sigma$ (i.e., $r_{ij} < r_c$). Using additional notations for the unit vector $\mathbf{e}_{ij} = (\mathbf{r}_i - \mathbf{r}_j)/r_{ij}$ and the relative velocity $\mathbf{v}_{ij} = \mathbf{v}_i - \mathbf{v}_j$, the pair forces in Eq. (S2) can be defined as follows:

$$\mathbf{F}_{ij}^{(C)} = a_{\alpha(i)\beta(j)}(1 - r_{ij}/\sigma)\mathbf{e}_{ij}\,, \tag{S3}$$

$$\mathbf{F}_{ij}^{(D)} = -\gamma\omega^{D}(r_{ij})(\mathbf{e}_{ij}\mathbf{v}_{ij})\mathbf{e}_{ij},\ \mathbf{F}_{ij}^{(R)} = (2\gamma k_B T)^{1/2}\omega^{R}(r_{ij})\theta_{ij}\mathbf{e}_{ij}. \quad \text{(S4)}$$

These equations include the following parameters and functions: $a_{\alpha\beta}$ is the maximum amplitude of the repulsion force between the pair of particles, $\gamma = 4.5m/\tau$ is the friction coefficient, ω^{D} and ω^{R} are the weight functions of the amplitudes of the random and the dissipative forces, and θ_{ij} is a random variable with zero mean and unit variance. According to Ref. [S4], there is the following relationship between the weight functions: $\omega^{D}(r_{ij}) = [\omega^{R}(r_{ij})]^2 = (1 - r_{ij}/\sigma)^2$. It is necessary to satisfy the fluctuation-dissipation theorem [S6] required to bring the system into thermodynamic equilibrium. Thus, the combination of the viscous frictional force and the random force ensures the correct thermostatting of the system under the *NVT* ensemble conditions. The conservative force $\mathbf{F}_{ij}^{(C)}$ in Eq. (S3) is purely repulsive; it takes into account the relationship between the DPD particles and the chemical structure of the corresponding molecular objects within the initial molecular system. It is determined by the force parameters a_{ij}.

To account for the structure of the polymer molecules and the shape of the nanoparticles, we introduce additional forces describing the bonds between the beads. They are determined by the following total potential energy

$$U = \sum_{i=1}^{N_{bonds}} U_i^{(bond)}(\mathbf{r}_{b(i,1)},\mathbf{r}_{b(i,2)}). \quad \text{(S5)}$$

In this equation, the functions $U_i^{(bond)}$ correspond to the energies of bond deformation between bonded DPD particles. N_{bonds} is the total number of bonds in the system. The vectors $\mathbf{r}_{b(i,1)}$ and $\mathbf{r}_{b(i,2)}$ are the positions of the particles corresponding to the i-th bond taken from the pair list $b(i,j)$ (i= 1, ..., N_{bond}, j = 1,2). The list $b(i,j)$ contains the numbers of the bonded particles. The potentials describing the bond deformations are harmonic:

$$U_i^{(bond)}(\mathbf{r}_{b(i,1)},\mathbf{r}_{b(i,2)}) = 1/2\, K_{\alpha(b(i,1))\beta(b(i,2))}\,(|\mathbf{r}_{b(i,1)} - \mathbf{r}_{b(i,2)}| - r_{0,\alpha(b(i,1))\beta(b(i,2))})^2. \quad \text{(S6)}$$

In these equations, $K_{\alpha\beta}$ and $r_{0,\alpha\beta}$ are the stiffness coefficients and bond length equilibrium values respectively. These coefficients are different for pairs of particles belonging to different subsystems of the model. In our case, α and β take the values A, B, and C (i.e., particles belonging to the polymer chain block A, block B, and nanoparticle, respectively).

It should be noted that, depending on the model of the molecular object, the potential energy may also contain other contributions, e.g. from the deformation of the angles between the valence bonds, torsion angles, etc., see Ref. [S5, S7].

All our simulations are performed using a parallel DPD code used in Ref. [S5, S7, S8].

S2. Additional information on the parameterisation of the polymer chain model and nanoparticles

To estimate the values of the parameters K_{NP}, h_{NP}, K_P, and h_P for which there are no "piercing" and "side-cutting" effects for the NP, we performed theoretical estimations using two simple models described in the following Sections S2.1 and S2.2. This was complemented by direct simulations using a relatively small system of A_5B_5 polymer chains and an NP with $M = 20$ ($20 \times 20 \times 1$ particles) placed in a cubic simulation cell with imposed periodic boundary conditions and an edge length of 14σ. The values of all $a_{\alpha\beta}$ were chosen to be equal to 25. The methodology for constructing the system (see Section 2.3) and performing the calculations is the same as the modelling methodology used for all the systems considered in the main text of this paper. Using this model, productive trajectories with a duration of $10^6 - 10^8$ DPD steps were generated and estimates were made for various characteristics of the NP, discussed below.

S2.1. Piercing effect estimation

To estimate the time for the polymer chain to pierce the NP (the "piercing" effect), we calculated a jump time $t(h)$. It is the time required for a probe bead to jump through a plane formed by beads ordered on a square lattice with step h, corresponding to the plate-like NP, see Figure S1a. The jump time is related to the potential barrier $U(h,l)$ created by the NP surface by the following equations:

$$t\,(h) = t_0 \exp\,(U(h,0)/k_B T), \tag{S7}$$

$$U(h,l) = \sum_{i=1}^{M}\sum_{j=1}^{M} U_2(((h \cdot i)^2 + (h \cdot j)^2 + l\,)^{1/2}), \tag{S8}$$

$$U_2\,(r) = \begin{cases} a(1-r)^2 / 2, r \le 1, \\ 0, r > 1, \end{cases} \tag{S9}$$

where i and j indicate the position of particles, and l is the distance of the probe particle relative to the centre of the square lattice. The settled lifetime t_0 was set equal to 1 DPD step. The lattice size M was chosen to be 20. The potential U_2 corresponds to the intermolecular interaction strength (S9). The value $a = 25$ was chosen as the smallest possible value in the

DPD parameterisation used [S1-S5, S7, S8]. A visual representation of the parameters described above is shown in Figure S1a. The parameter h was varied in the range from 0.3σ to 0.68σ. The estimated jump time of the probe particle through the potential barrier $U(h,l)$ (see Eq. (S8)) is shown in Figure S1b. According to the obtained data, when h = 0.5σ, the jump time is estimated to be ~10^{11} DPD steps, which is significantly longer than usually used when studying the behaviour of coarse-grained models [S1–S5].

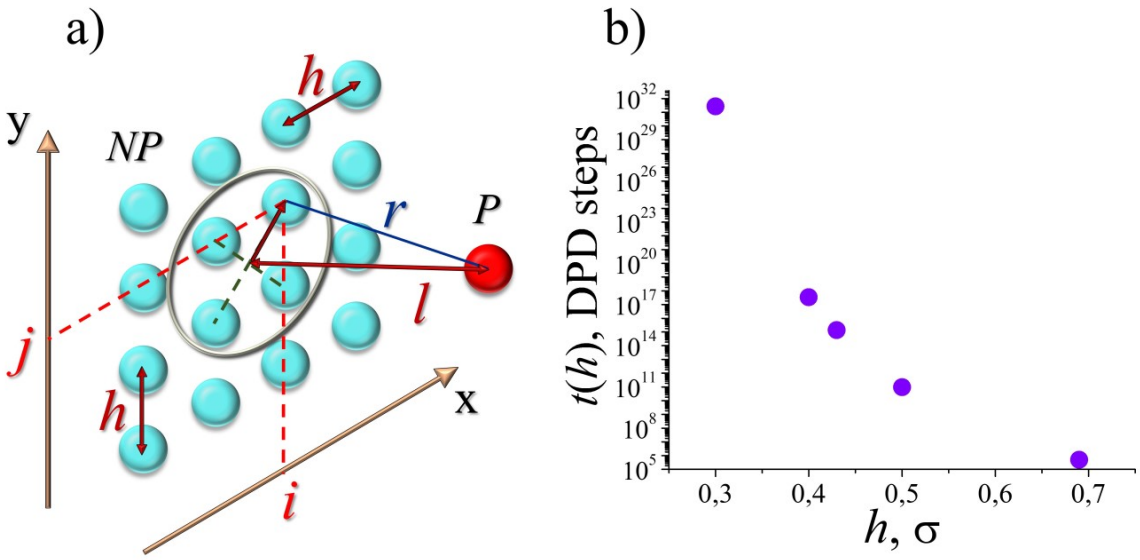

Figure S1. a) Visual representation for the parameters in Eqs. (S7)–(S9). b) The jump time of the probe particle through the potential barrier $U(h,l)$.

S2.2. Side-cutting effect estimation

To estimate the time for the polymer chain to cut through the NP from the side (the "side-cutting", we calculated the passage time $t(h,b)$ of a pair of probe particles separated by a distance b along the NP plane while maintaining the distance between them. The beads of the NP as in Section 2.1 are ordered on the square lattice with step h. The following equations are used for $t(h,b)$ and the potential barrier $U(h,b,l)$ created by the NP model surfaces:

$$t(h,b) = t_0 \exp\left(U(h,b,0)/k_B T\right), \tag{S10}$$

$$U(h,b,l) = \sum_{i=1}^{M}\sum_{j=1}^{M} U_2(((h \cdot i\text{-}l)^2 + (h \cdot j)^2 + (b/2)^2)^{1/2}). \tag{S11}$$

The potential U_2 is defined by Eq. (S9). A visual representation of all the parameters described above is shown in Figure S2a. The settled time t_0 (see Eq. (S10)) was also set to 1 DPD step as in the previous model (see Section S2.1). The parameter h was varied in the range from 0.1σ to 0.68σ, while the parameter b was varied in the range from σ to 1.8σ. The

lower limit of b was chosen because this value is commonly used as the equilibrium bond length in DPD. The estimated passage time of the pair of probe particles through the potential barrier $U(h,b,l)$ (see Eq. (S11)) is shown in Figure S2b.

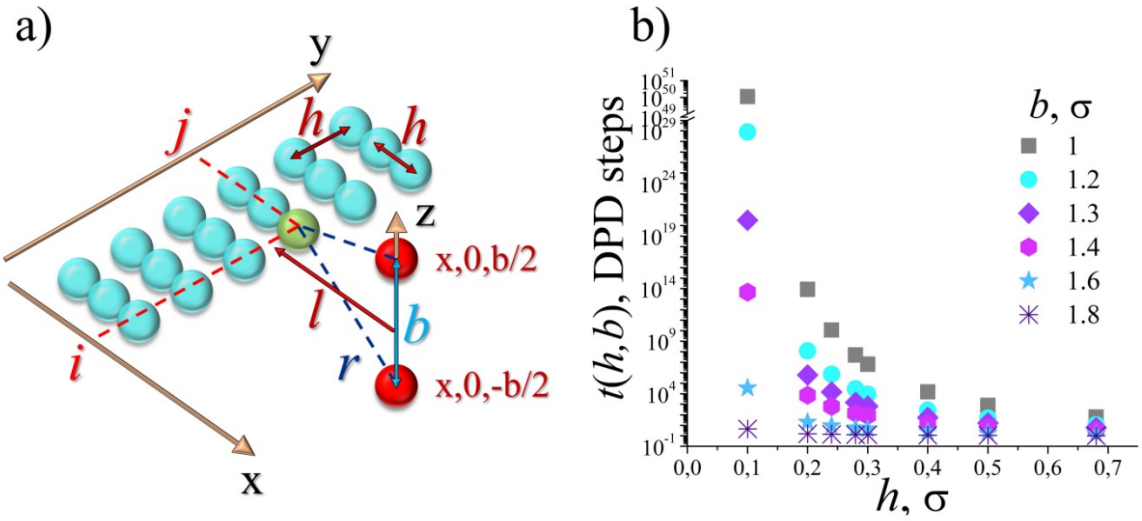

Figure S2. a) Visual representation of the parameters in Eqs. (S9)-(S11). b) The passage time of the pair of probe particles through the potential barrier $U(h,b,l)$.

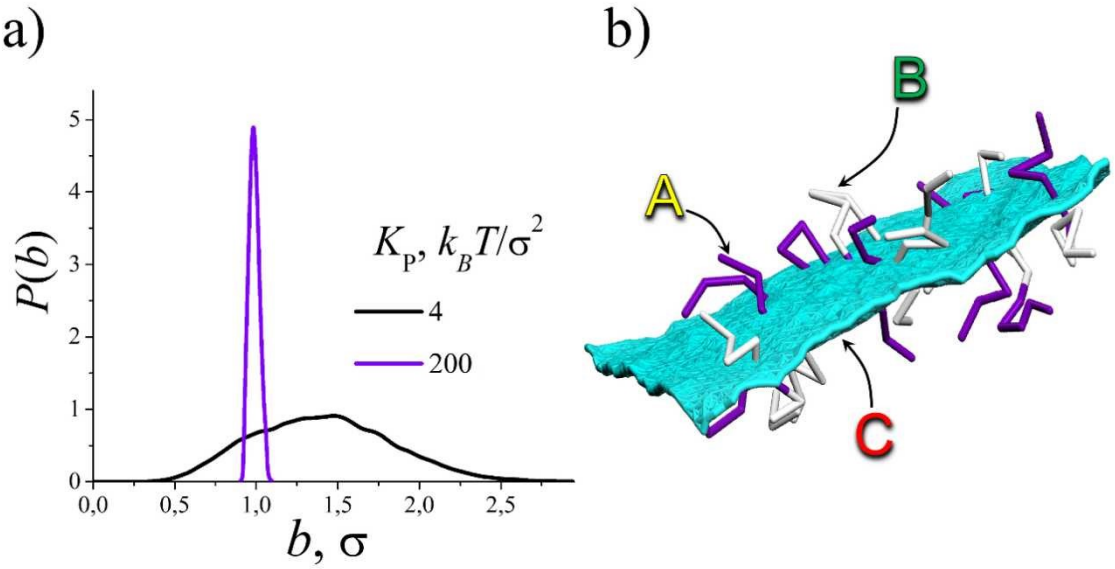

Figure S3. a) Probabilities of the distribution of bond lengths b in polymer chains for different values of the stiffness coefficient K_P obtained by direct simulations (see beginning of Section 2). The average bond lengths are 1.4σ when $K_P = 4\ k_BT/\sigma^2$, and σ when $K_P = 200\ k_BT/\sigma^2$. $h_P = \sigma$, $K_{NP} = 600\ k_BT/\sigma^2$, $h_{NP} = 0.2\sigma$. b) An example of the side-cutting effect of the NP by the polymer chains at $K_P = 4k_BT/\sigma^2$, $h_P = \sigma$, $K_{NP} = 600\ k_BT/\sigma^2$, $h_{NP} = 0.2\sigma$. The picture shows the chains stuck in the NP.

Additionally, trial simulations of the nanocomposite model described at the beginning of Section S2 with various values of K_P ($K_P = 4k_BT/\sigma^2$ or $K_P = 200k_BT/\sigma^2$), $h_P = \sigma$, $K_{NP} =$

600 k_BT/σ^2, h_{NP} = 0.2σ were performed (the choice of these parameters is discussed in Section 2.3). Note that in simulations the values of b and h could change and the average bond lengths between the beads in the polymer chains, $<b>$, and the NP, $<h>$, were calculated. As can be seen in Figure S3a, at $K_P = 4k_BT/\sigma^2$ the average bond length between particles in the polymer chains $<b> \approx 1.4\sigma$. Thus, according to Figure S2b, a pair of particles with such relative big bond length can move along the NP surface prepared with $h = 0.5\sigma$ (see the previous section) in times of the order of only 10 DPD steps. An example of the side-cutting effect of the NP by the polymer chains is shown in Figure S3b. If we choose $K_P = 200k_BT/\sigma^2$ as in Ref. [S5], the direct simulation give for the polymer chains $<b> \approx \sigma$ (see Figure S3a). In this case, according to Figure S2b, values of h less than 0.3σ can be used to be sure that the side-cutting effect does not occur during long simulation times (> 10^8 DPD steps). According to Figure S1b, such values of h also can be used to be sure that the piercing effect does not occur at least during 10^{31}–10^{32} DPD steps.

S2.3. Selecting bond strain potential parameters for polymer chain and NP

To select the bond strain potential parameters, we performed direct simulations of the nanocomposite model described at the beginning of Section S2. Wherein, for the polymer we used the parameters approved in the previous section, $K_P = 200k_BT/\sigma^2$, $h_P = \sigma$, and for the NP different combinations of parameters were checked: K_{NP} varied within the range from $100k_BT/\sigma^2$ to $800k_BT/\sigma^2$, and h_{NP} was equal to 0.1σ, 0.2σ, or 0.4σ. Figure S4 shows how the average bond length in the NP $<h>$ varies with K_{NP} and h_{NP}. The increase in the average bond length $<h>$ with respect to the equilibrium bond length h_{NP} is explained by the effect of the swelling of the NP model due to the strong mutual repulsion between the beads in their composition as a result of their high-density packing. This leads to the appearance of large conservative force gradients and, as a consequence, particle accelerations. In such cases, it is necessary to reduce the integration step to stabilise the scheme for integrating the equations of motion (Eqs. (S1), (S2)). Test simulations have shown that relatively large integration steps (0.02τ) can be used in our model for $K_{NP} < 800\ k_BT/\sigma^2$.

In order to maintain a relatively large integration step and to satisfy the condition of the previous section that the values of h should be less than 0.3σ (to avoid the piercing and side-cutting effects), we chose the following bond strain potential parameters: K_P = 200 k_{BT}/σ^2, $h_P = \sigma$ for the polymer chain (as in ref. [S5]); and K_{NP} = 600 k_{BT}/σ^2, $h_{NP} = 0.2\sigma$ for the NP. In this case, as can be seen from Figure S4, the average length of the lateral bonds $<h>$ in the NP tends to saturate around ≈ 0.28σ. For $b = \sigma$ and $h = 0.28\sigma$, according to Figure S2b,

the side-cutting effect can occur in a time greater than 10^8 DPD steps, which is beyond the maximum simulation time used in this study.

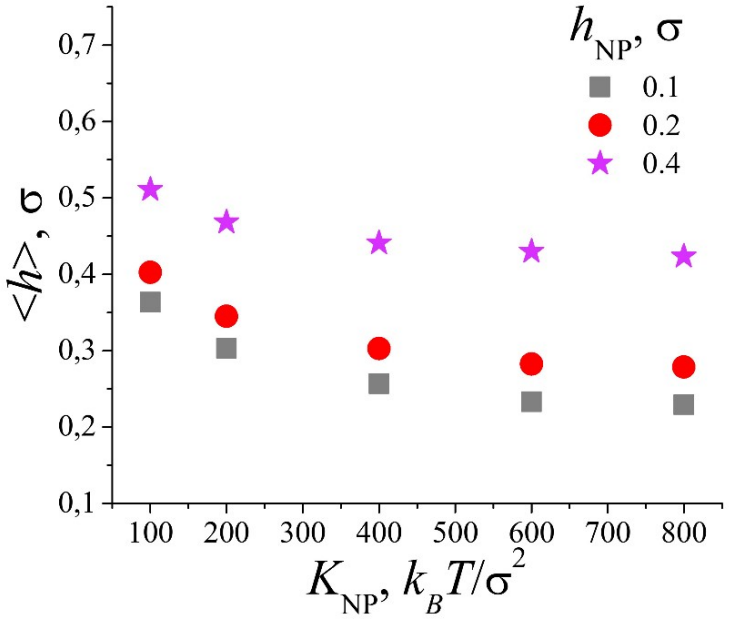

Figure S4. The average length of longitudinal and transverse bonds in the NP model as a function of K_{NP} and h_{NP}. $K_P = 200k_BT/\sigma^2$, $h_P = \sigma$.

S2.4. Verification of the selected values of the parameters of the bond strain potentials

Since the correct modelling of the microphase separation requires excluding the interaction of the polymer particles located on opposite sides of the NP plane, we evaluated the closest distance between the polymer and the NP beads. To determine this value, we calculated the probability $P(r)$ of finding beads of type A and B at a distance r from the NP beads (type C) using the following equation:

$$P(r) = 1 / N_P / N_{NP} \sum_{j=1}^{N_{NP}} \sum_{i=1}^{N_P} \delta(|\mathbf{r}_{ij}| - r), \quad \text{(S12)}$$

where N_P and N_{NP} are the numbers of the polymer and the NP beads, $\mathbf{r}_{ij}$ is the vector between the centres of the *i-th* and *j-th* particles.

The calculations were performed using the model described at the beginning of Section S2. h_{NP} was varied in range from 0.1σ to 0.5σ. The productive run consisted of 10^8 DPD steps. The results are shown in Figure S5. It can be seen that at $h_{NP} = 0.2\sigma$ the closest approach distance is 0.6σ. This means that particles of polymer chains located on opposite sides of the NP can approach each other at a distance of 1.2σ, which, according to the

definition of the force in Eq. (S2), eliminates the interaction of polymer chains separated by a nanoparticle.

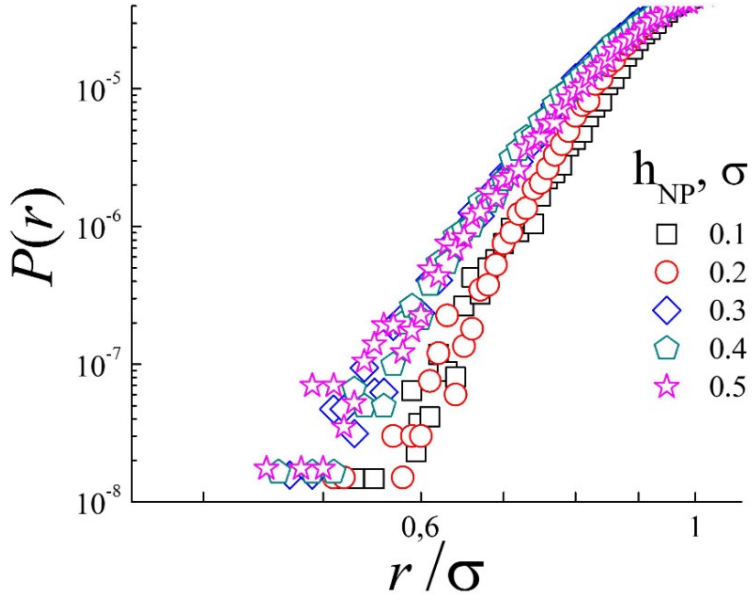

Figure S5. Probabilities $P(r)$ of finding A and B beads at distance r from C beads at different h_{NP}. The figure shows the $P(r)$ for $r < \sigma$. $K_P = 200k_BT/\sigma^2$, $h_P = \sigma$, $K_{NP} = 600k_BT/\sigma^2$.

Also during this calculation, the occurrence of piercing and side-cutting effects of the NP by polymer chains was periodically monitored. No such effects were found at the simulation times achieved.

S3. NP shape control

To control the shape stability of the NP, the squared radius of gyration R_g^2 were first calculated for fixed polymer chain properties (A_5B_5, $K_P = 200\ k_BT/\sigma^2$, $h_P = \sigma$) and different values of K_{NP} and h_{NP}. K_{NP} varied within the range from $100k_BT/\sigma^2$ to $800k_BT/\sigma^2$, and h_{NP} was equal to 0.1σ, 0.2σ, or 0.4σ. Figure S6a shows an example of the behaviour of R_g^2. It can be seen that the NP is a labile object. According to Figure S6b, the radius of gyration decreases as the equilibrium bond length h_{NP} decreases and the bond stiffness K_{NP} increases. Together with this, the NP dimension tends to stabilise due to the balance between the total bond deformation forces and the repulsive forces between closely packed particles.

To monitor the stiffness of the NP plate for each row of beads in two lateral directions, since these rows can be treated as separate chains, we introduced the following characteristics: contour lengths $L_{1,i}$ and $L_{2,j}$ and end-to-end vectors $\mathbf{R}_{ee1,i}$ and $\mathbf{R}_{ee2,j}$, see Figure 2a. The average values $<L_1>$ and $<L_2>$ were calculated by averaging over each of the directions and over 10,000 instantaneous NP configurations obtained during the productive

run of 10^6 DPD steps (we use the model described at the beginning of Section S2). Similarly, the average values of $<\mathbf{R}^2_{ee1}>$ and $<\mathbf{R}^2_{ee2}>$ have been obtained, allowing us to calculate the average Kuhn segments [S9, S10] for particle rows belonging to the "*transverse*" and "*longitudinal*" directions of the NP plate as $b_{k1} = <\mathbf{R}^2_{ee1}>/<L_1>$ and $b_{k2} = <\mathbf{R}^2_{ee2}>/<L_2>$. By analogy with C_∞ for the polymer chain [S9, S10], we now introduce a statistical stiffness C_{2D} of the NP plate:

$$C_{2D} = (b_{k1} + b_{k2})/\ 2<h>, \tag{S13}$$

where $<h> = (<L_1> + <L_2>)/2M$. The plots of C_{2D} as a function of K_{NP} and h_{NP} are shown in Figure 2b. It can be seen that the stiffness of the NP plate increases with decreasing h_{NP}. And as K_{NP} increases for each h_{NP}, the C_{2D} values tend to saturate. The results obtained confirm the choice of the parameters of the bond deformation potential and allow us to consider the generated NP model as an object that maintains its flat shape.

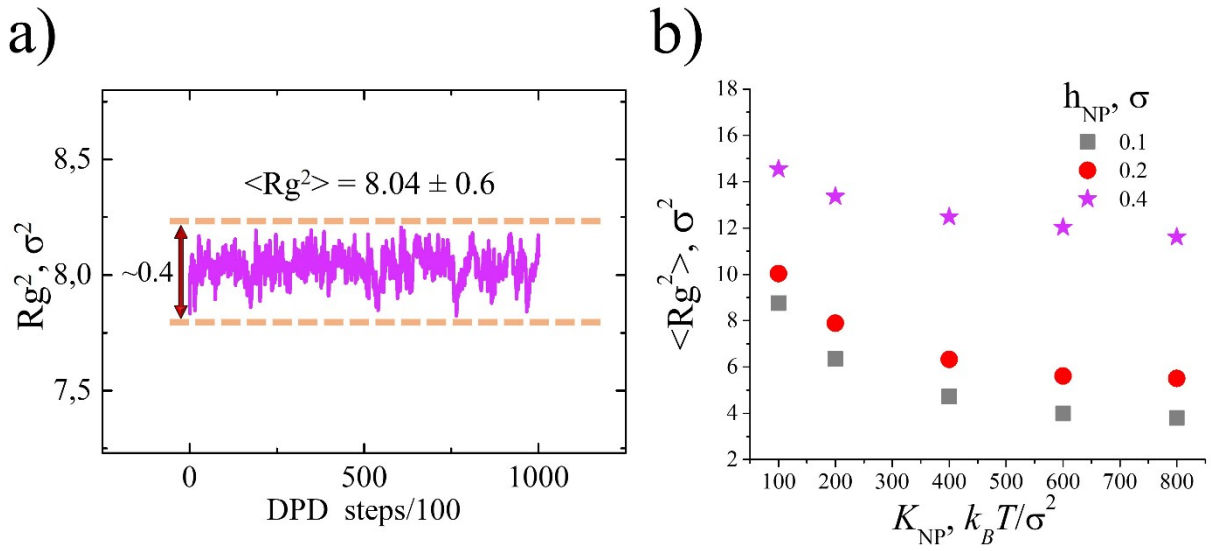

Figure S6. a) An example of the evolution of the NP squared radius of gyration (K_P = 200 k_BT/σ^2, $h_P = \sigma$, K_{NP} = 200 k_BT/σ^2 and $h_{NP} = 0.2\sigma$). b) Average value of the squared radius of gyration as a function of K_{NP} and h_{NP}. $K_P = 200k_BT/\sigma^2$, $h_P = \sigma$.

S4. Control of the internal structure of the material model

S4.1. Static structural factor

To characterise the internal structure of the system, Figure S7a, we have calculated the partial static structure factor $S_\alpha(q)$ for particles of type α = A, B as the Fourier transform of the local density $\rho_\alpha(r)$ of the beads in the simulation cell [S11], Figure S7b, as follows:

$$S_\alpha(q) = \int\int_{|\mathbf{q}|=q} <\rho_\alpha(\mathbf{r})\exp(i\mathbf{q}\cdot\mathbf{r})> d\Omega d\mathbf{r}. \tag{S14}$$

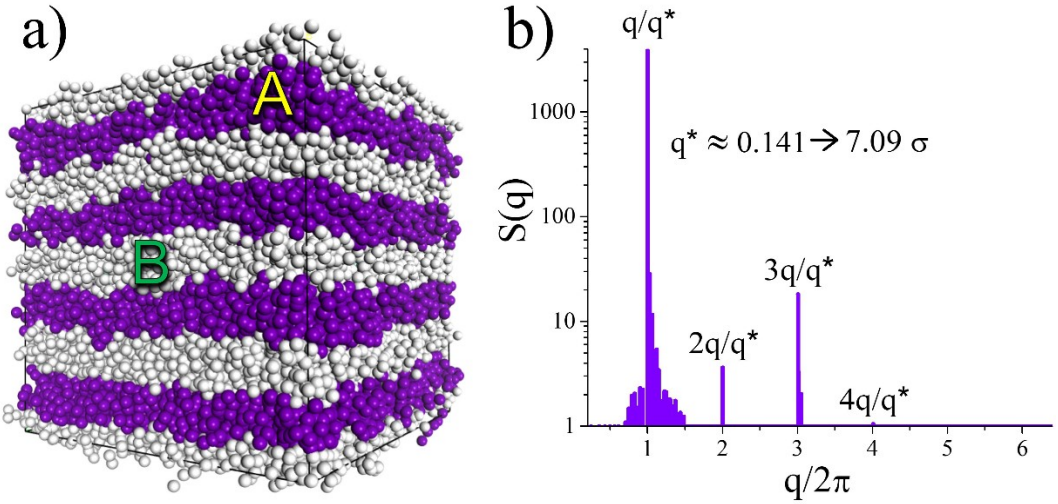

Figure S7. a) Visualisation of domains formed by particles of type A and B when a_{AB} = 40. The size of the simulation cell L = 28.17σ is chosen so that the domains are parallel to the cell faces. b) Structural factor (S14) for this system showing that the period of the emerging lamellae is ≈ 7.09σ.

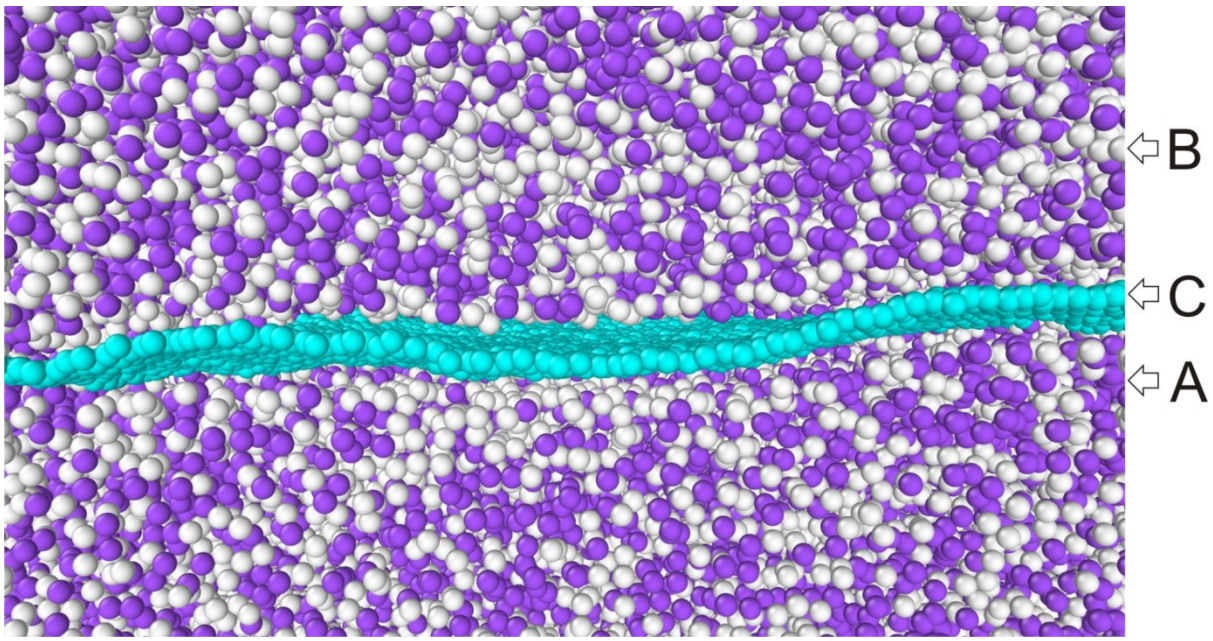

Figure S8. Snapshot of the local distribution of polymer particles near the NP surface. It was taken in the productive part of the trajectory after $1.5 \cdot 10^6$ DPD steps. The interaction parameters are $a_{AB} = a_{BC} = 25$, $a_{AC} = 40$. To improve visibility, the bonds between the particles are not shown and the diameter of the beads is also reduced.

S4.2. Polymer density distribution relative to NP surface

The property of the local order of the polymer beads relative to the NP surface is studied based on the density distribution $\rho_\alpha(z)$ (z is the distance from the NP surface). The main difficulty in calculating this property is that the NP surface undergoes short and long-term oscillations, which can be seen in Figure S6a, showing the time evolution of the squared

radius of gyration. It can also be seen in the instantaneous snapshot shown in Figure S8. As we could not find any ready-made algorithms for calculating the density distribution relative to a moving surface, we developed our calculation procedure.

We calculate the density distribution for particles of type A and B during the productive run as the average of the instantaneous density:

$$\rho_\alpha(z) = 1/N_{\text{surf}}/N'_\alpha \sum_{j=1}^{N_{surf}} \sum_{i=1}^{N'_\alpha} \delta(|(\mathbf{n}_j\mathbf{r}_{ij})|-z)\cdot\delta(|\mathbf{r}_{ij}-(\mathbf{n}_j\mathbf{r}_{ij})\mathbf{n}_j|-r_{\text{out}}). \quad \text{(S15)}$$

In this expression, $N_{\text{surf}} = (M-2)^2$ is the number of particles in the NP, excluding particles at the boundaries (see Figure S9). At the centres of these particles, local surface normals $\mathbf{n}_j$ to the NP surface are constructed. The set N'_α contains all particles of type α for which the distance $|d\mathbf{r}_{ij}| = |\boldsymbol{r}_{ij}-(\boldsymbol{n}_j\boldsymbol{r}_{ij})\boldsymbol{n}_j|$ from the normal is less than the cut-off radius r_{out}, see Figure S9. The maximum z value was set to half the edge size of the simulation cell. Since the normals $\mathbf{n}_j$ are introduced at each point of the surface, the direction of which is determined by the instantaneous local curvature of the NP surface, it is possible to select layers of polymer beads at a distance z from the surface for each moment of time. In this case, the geometry of the layers is determined by the instantaneous geometry of the NP surface.

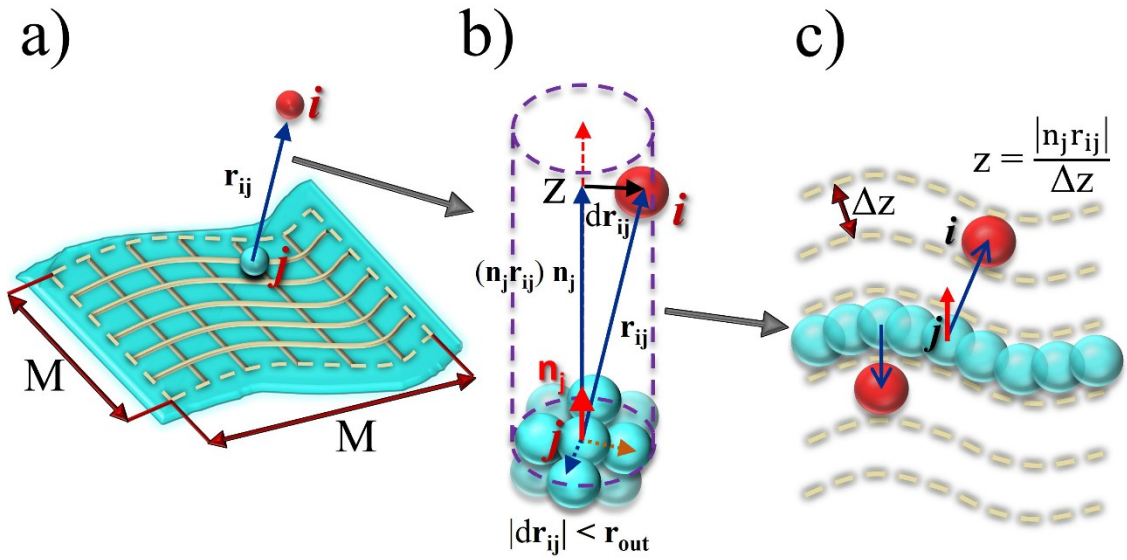

Figure S9. Explanation of the procedure for calculating the distribution density of polymer particles relative to the NP surface. Schematic representations are shown for a) NP (the dotted line marks the rows of beads that are not included in the density distribution calculations); b) the local normals, $\mathbf{n}_j$, to the surface at the j–th bead, the relative position vector $\mathbf{r}_{ij}$, and its projection: $(\mathbf{n}_j\mathbf{r}_{ij})\mathbf{n}_j$, on the direction of the normal $\mathbf{n}_j$, and $d\mathbf{r}_{ij}$ on the radial direction from the normal n_j to the i-th bead; c) the layer of particles located at distance z from the NP surface.

S5. Additional images of different states of the nanocomposite

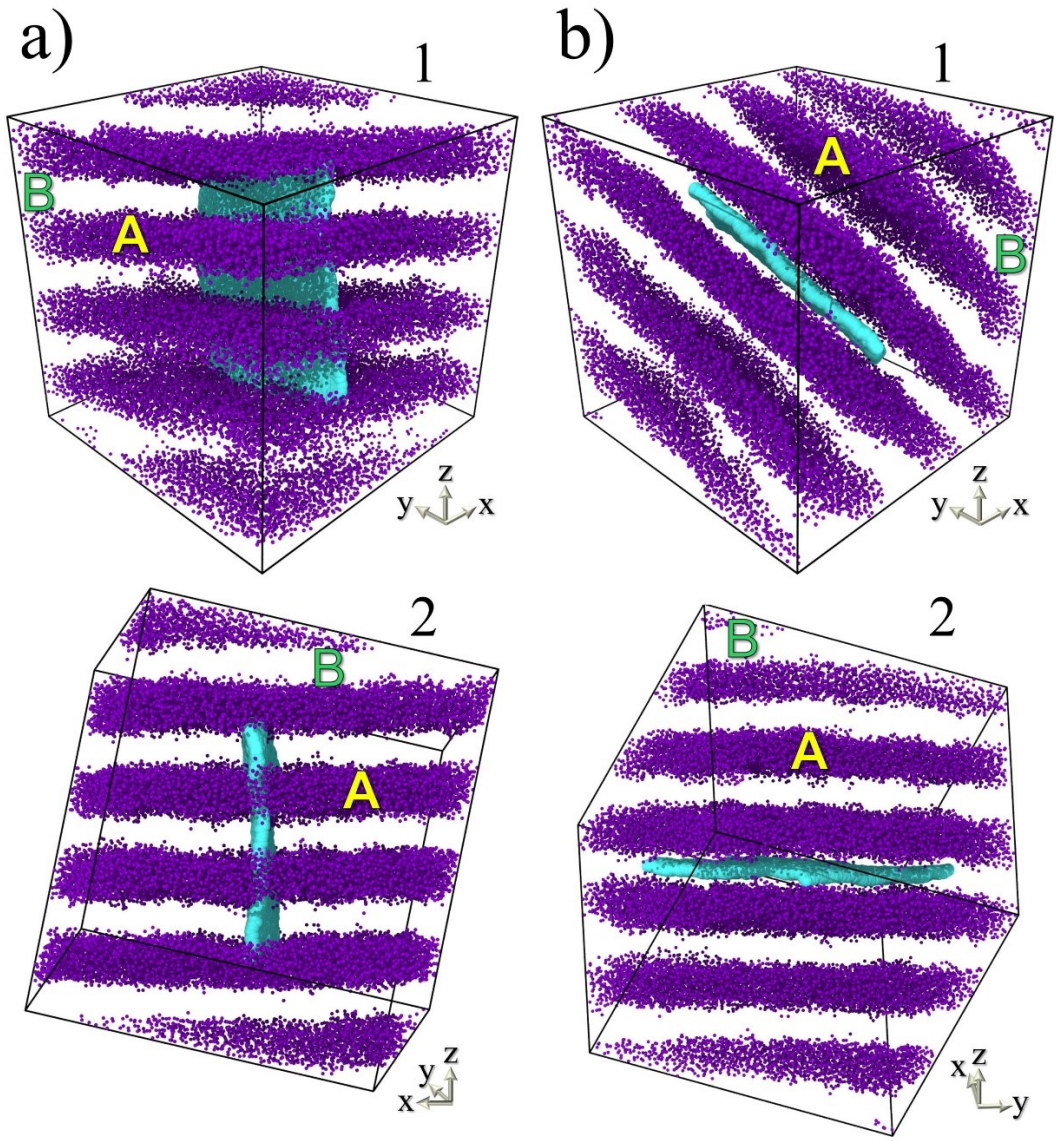

Figure S10. Examples of the NP orientation relative to polymer matrix domains were obtained for a_{AC} = 30, a_{BC} = 25, and a_{AB} = 33. The systems shown in figures (a) and (b) were obtained for two statistically independent states. For better visualisation, type B beads have been removed from the simulation cell. The numbers indicate different orientations of the simulation cells: 1 - isometric projections, 2 - plane of polymer domains is horizontal.

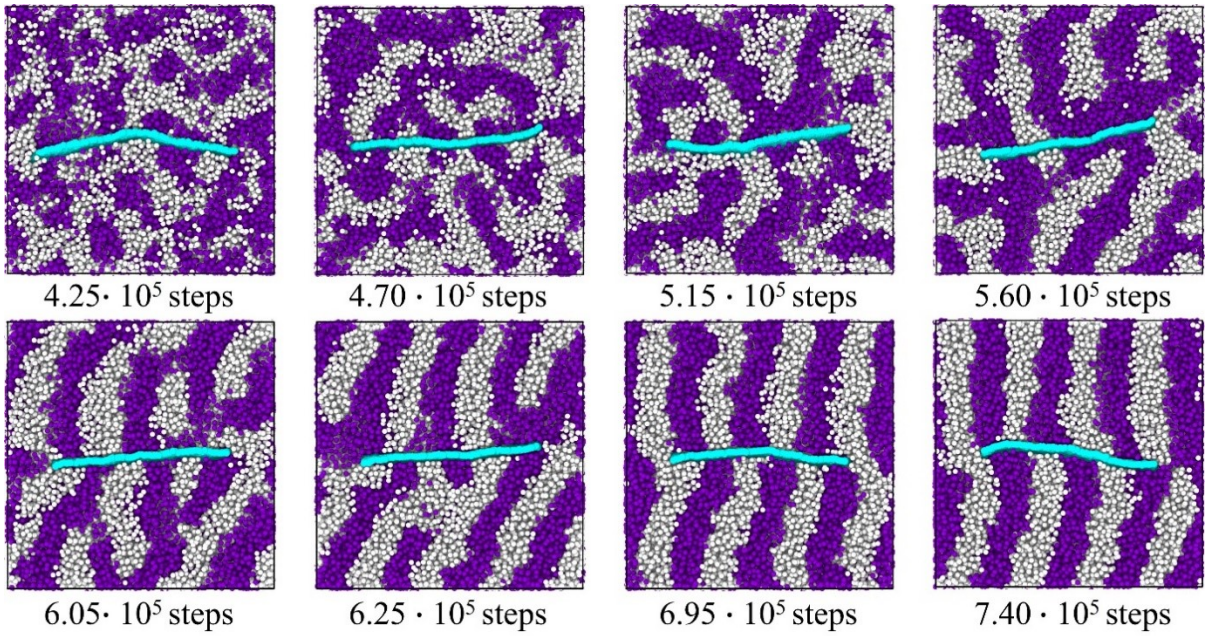

Figure S11. Dynamics of structural ordering in the nanocomposite at simulation times ranging from $4.25 \cdot 10^5$ to $7.40 \cdot 10^5$ DPD steps when $a_{AB} = 40$, $a_{AC} = 25$, $a_{BC} = 25$. The size of a simulation cell is 30.17σ. For visualisation, a cross-section of the simulation cell was made by a plane passing through its centre. The color scheme is the same as in Figure S10.

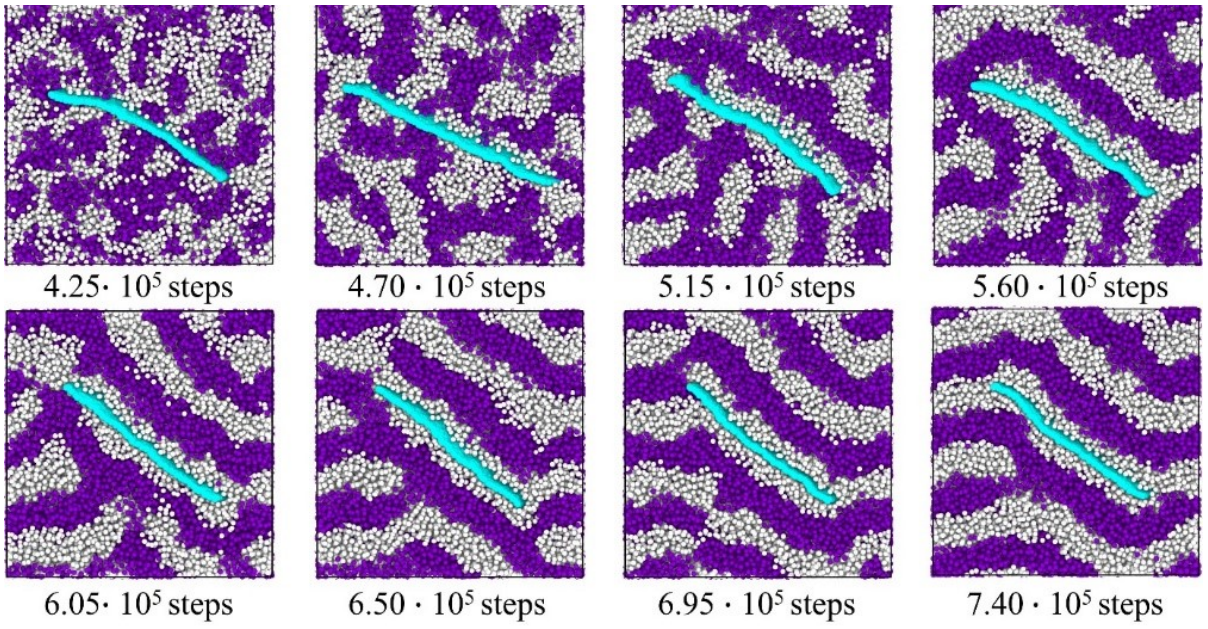

Figure S12. The dynamics of structural ordering in the nanocomposite at simulation times ranging from $4.25 \cdot 10^5$ to $7.40 \cdot 10^5$ DPD steps when $a_{AB} = 40$, $a_{AC} = 40$, $a_{BC} = 25$. The color scheme is the same as in Figure S10.

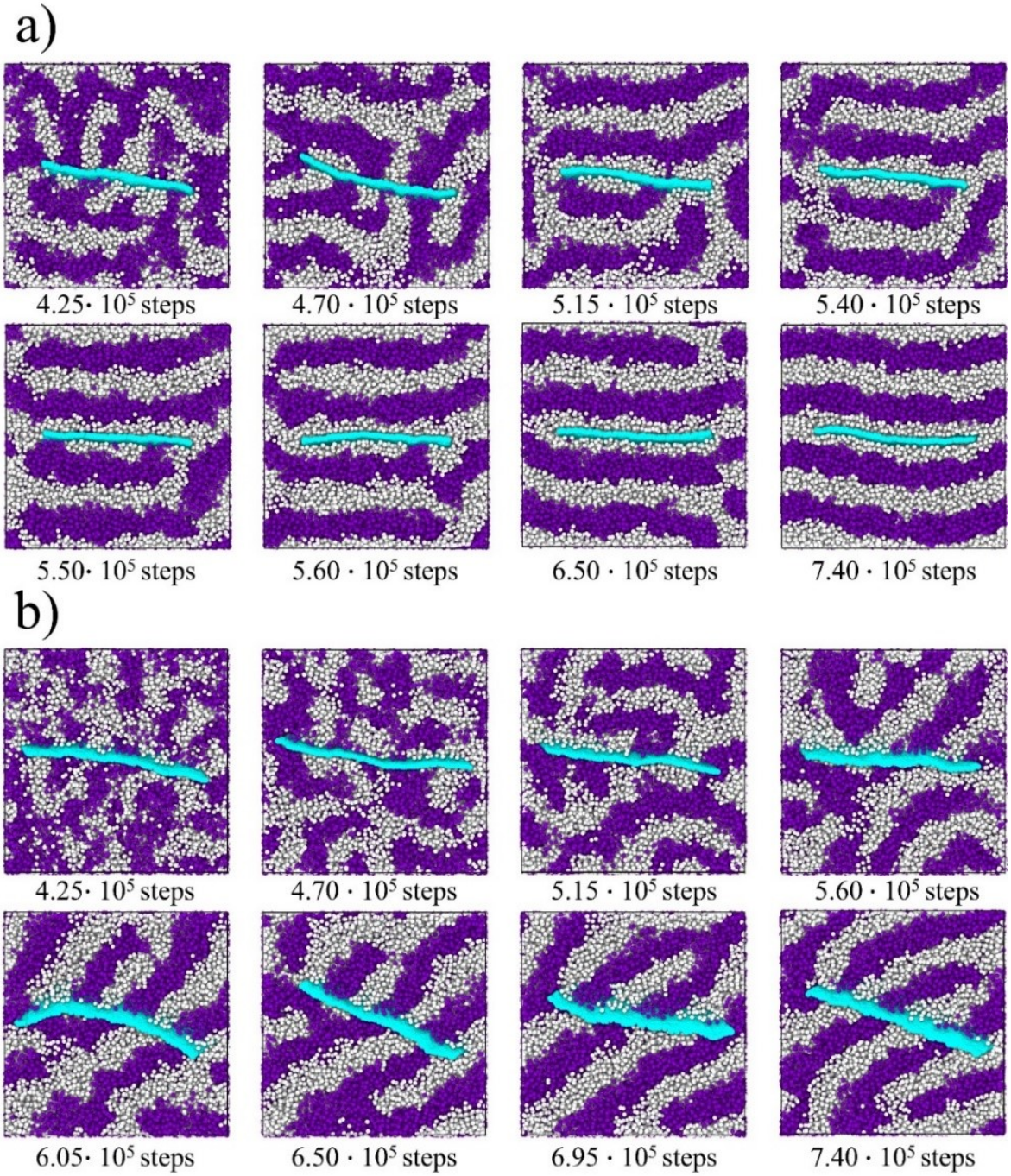

Figure S13. Dynamics of structural ordering in the nanocomposite at simulation times ranging from $4.25 \cdot 10^5$ to $7.40 \cdot 10^5$ DPD steps when $a_{AB} = 40$, $a_{AC} = 33$, $a_{BC} = 25$. Image sets a) and b) were obtained for two statistically independent starts. The color scheme is the same as in Figure S10.

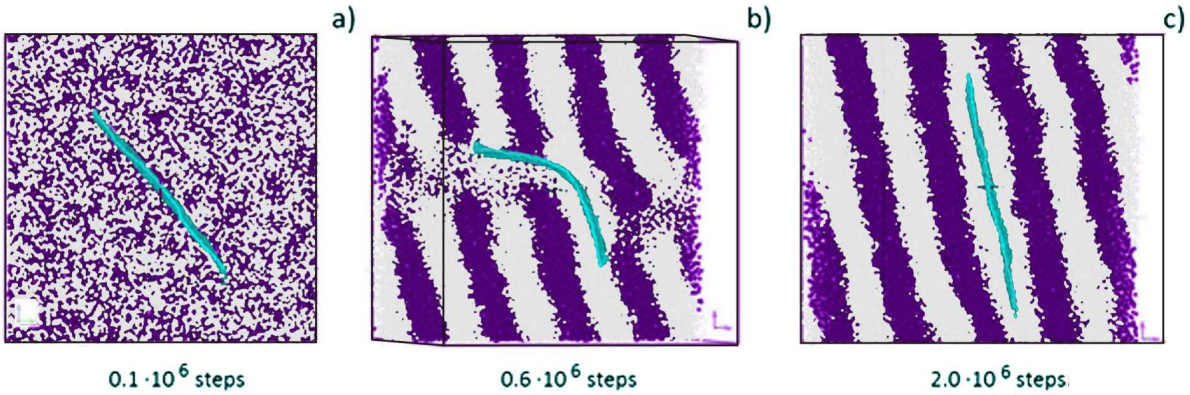

Figure S14. An example of the formation of a transient unstable state of the NP when a_{AB} = 34, a_{AC} = 40, and a_{BC} = 25. The color scheme is the same as in Figure S10.

S6. Nanoparticle mutual order control

To control the ordering of the flat nanoparticles, we calculated their mutual orientational order parameter (OOP) [S5,S12] using the mean value of the second Legendre polynomial

$$S = (3 \langle \cos^2\theta \rangle - 1) / 2, \qquad \text{(S16)}$$

where θ is an angle between the normals passing through the centre of the nanoparticle surfaces. The brackets indicate the averaging over the instantaneous states of all nanoparticle pairs. These states are taken every 1000 DPD steps in the productive trajectory. The order parameter can vary from 0.5 to 1. If all 2D NPs are aligned parallel to each other, then S ≈ 1. Note that the order parameter has been calculated only for cases where several nanoparticles are present in the system. The OOP for the nanoparticle and the lamellae was not calculated because the interface between the lamellae formed by the polymer chains is very blurred, which makes the implementation of the calculation of the normal to such a surface an ill-defined problem.

The results obtained are shown in Figure 8b. As can be seen, $S > 0.7$ for cases where the NP plane is perpendicular to the plane of the lamellae (Figure S10a) and parallel to them (Figure S10b). In other words, the NP planes are well aligned. In this case, the degree of ordering for NPs incorporated into a domain is significantly higher ($S = 0.91 \pm 0.06$) than for nanoparticles perpendicular to the domains ($S = 0.84 \pm 0.14$). This means that in the first case the domain boundary has a stabilising effect on the orientation of the NPs. In the second case, the NPs have a significant degree of freedom. The interesting order, when one NP is embedded in domain B and the second is oriented perpendicular to the domains, has $S = -$

0.35 ± 0.14, indicating their perpendicular arrangement. This shows that the second nanoparticle has an orientation perpendicular to the domains of the polymer matrix.

References

S1. R. D. Groot and P. B. Warren, *J. Chem. Phys.*, 1997, **107**, 4423–4435.

S2. P. J. Hoogerbrugge and J. M. V. A. Koelman, *Europhysics* Letters, 1992, **19**, 155–160.

S3. J. M. V. A. Koelman and P. J. Hoogerbrugge, *Europhysics* Letters, 1993, **21**, 363–368.

S4. P. Español and P. Warren, *Europhysics* Letters, 1995, **30**, 191–196.

S5. P. V. Komarov, P. G. Khalatur and A. R. Khokhlov, *Polym Adv Technol.,* 2021, **32**, 3922–3933.

S6. M. Doi and S. F. Edwards, *The Theory of Polymer Dynamics*, Oxford: Clarendon, 1986.

S7. V. Yu. Rudyak, A. A. Gavrilov, D. V. Guseva, S.-H. Tung and P. V. Komarov, *Mol. Syst. Des. Eng*., 2020, **5**, 1137-1146.

S8. A. A. Gavrilov, A. V. Chertovich, P. G. Khalatur and A. R. Khokhlov, *Macromolecules*, 2014, **47**, 5400–5408.

S9. E. F.Casassa and G. C. Berry, In: *Comprehensive Polymer Science and Supplements*; Elsevier, 1989; 71–120.

S10. M. Rubinstein and R. H. Colby, *Polymer Physics*; Oxford University Press, 2003.

S11. D. A. Kenn, *J. Appl. Crystallogr*., 2001, **34**, 172-177.

S12. J. J. Hermans, P. H. Hermans, D. Vermaas and A. Weidinger, *Recl. Trav. Chim. Pays-Bas*, 1946, **65**, 427–447.